NANO LETTERS

2007
Vol. 7, No. 7
2020−2023

High-Resolution Three-Dimensional Mapping of Semiconductor Dopant Potentials

Alison C. Twitchett-Harrison,* Timothy J. V. Yates, Simon B. Newcomb,† Rafal E. Dunin-Borkowski, and Paul A. Midgley

Department of Materials Science, University of Cambridge, Pembroke Street, Cambridge, CB2 3QZ, United Kingdom

Received April 12, 2007

ABSTRACT

Semiconductor device structures are becoming increasingly three-dimensional at the nanometer scale. A key issue that must be addressed to enable future device development is the three-dimensional mapping of dopant distributions, ideally under "working conditions". Here we demonstrate how a combination of electron holography and electron tomography can be used to determine quantitatively the three-dimensional electrostatic potential in an electrically biased semiconductor device with nanometer spatial resolution.

In an extrinsic semiconductor structure that contains local variations in dopant distribution, it is essential to be able to map the electrically active regions quantitatively to characterize the device function.[1,2] The electrical properties of nanoscale semiconductor structures are strongly dependent on the presence of interfaces and surfaces. Near such features, the electrical properties of the semiconductor may deviate substantially from its bulk properties. Many semiconductor characterization techniques, for example, scanning probe microscopies, either have poor spatial resolution or probe only the near-surface region of the device, which is sensitive to environmental conditions and surface damage. Off-axis electron holography is a transmission electron microscope (TEM) based interference technique that has been highlighted as a promising quantitative dopant profiling technique with the high spatial resolution that is required for the characterization of current and future device generations.[3] Electron holography is used to measure the phase change experienced by a high-energy electron wave passing through a thin specimen prepared from a semiconductor device. When acquired using an unperturbed vacuum wave and reconstructed using a reference hologram, the phase change can be related directly to the electrostatic potential distribution in the specimen. Here we show that by acquiring a series of off-axis electron holograms over a range of specimen tilt angles, tomographic reconstruction methods[4] can be used to measure quantitatively the three-dimensional electrostatic potential in a semiconductor device. We illustrate the approach by characterizing a focused ion beam (FIB) milled Si p−n junction in which the variation in the electrical properties of the device close to the surfaces of the specimen is of interest.[5]

The site-specific preparation of semiconductor devices for examination using electron holography can, at present, only be satisfied currently by FIB milling. In recent years, combined scanning electron microscope (SEM) and FIB workstations have provided increased flexibility and improved efficiency in the preparation of site-specific TEM specimens containing device structures.[6,7] However, the preparation of specimens using a high-energy ion beam creates amorphous regions at the semiconductor surfaces,[8,9] and the impact of the Ga ion beam on the electrical properties of the subsurface is not yet fully understood.

An FEI 200 FIB workstation operated at 30 kV with a Ga ion beam was used to prepare a thin, parallel-sided membrane of a Si p−n junction device in a novel geometry, as illustrated in Figure 1a. This geometry allows high specimen tilt angles to be achieved in the TEM without shadowing of the specimen by either the support grid or the surrounding specimen. The device comprised a 2.5 μm layer of 5×10^{18} cm^{-3} (nominal) B-doped (p-type) Si grown epitaxially on a 3×10^{18} cm^{-3} (nominal) Sb-doped (n-type) Si substrate. The crystalline specimen thickness was measured to be 330 ± 10 nm using convergent beam electron diffraction.[10] The sample was mounted in a cartridge[11,12] that enabled easy transfer between the FIB workstation and a special TEM specimen holder (Figure 1b), which was used to achieve high specimen tilt while simultaneously allowing an electrical bias to be applied to the FIB-prepared semiconductor specimen in the electron microscope.[11,12] Off-axis electron holograms

* Corresponding author. E-mail: act27@cam.ac.uk.
† Glebe Laboratories, Newport, County Tipperary, Ireland.

10.1021/nl070858n CCC: $37.00
Published on Web 06/12/2007

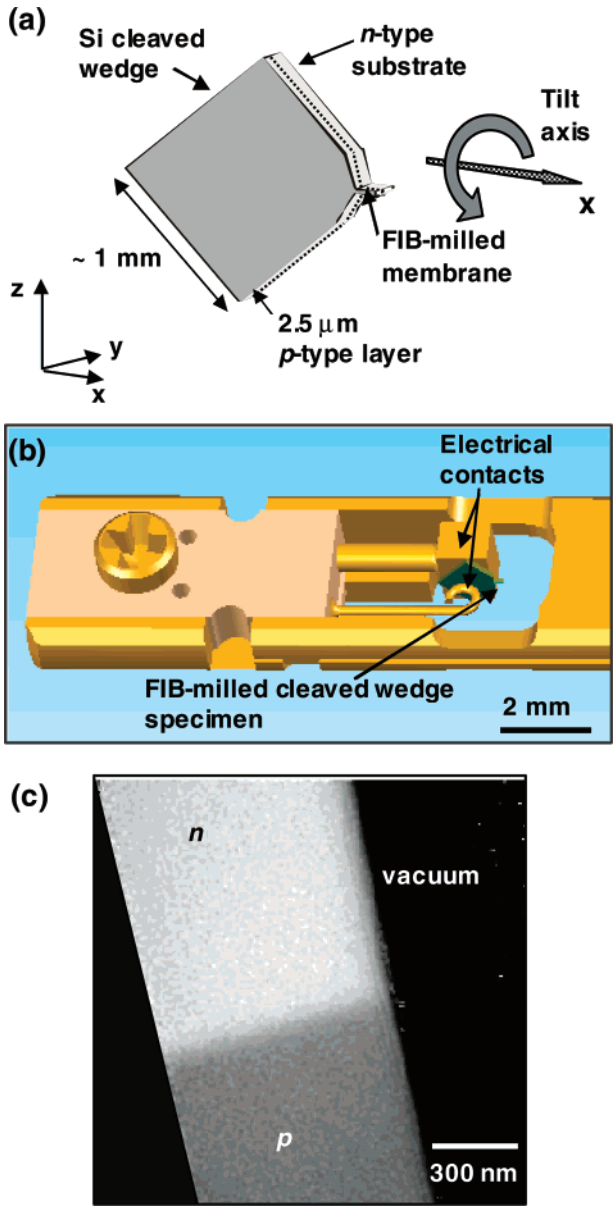

Figure 1. (a) Schematic diagram illustrating the specimen geometry used for electrically biased tomographic holography. (b) Design drawing of the two-contact electrical biasing TEM specimen holder. (c) Unwrapped reconstructed phase image (acquired at a specimen tilt angle of +20°) showing the phase variation across the p−n junction under a 3 V applied reverse electrical bias.

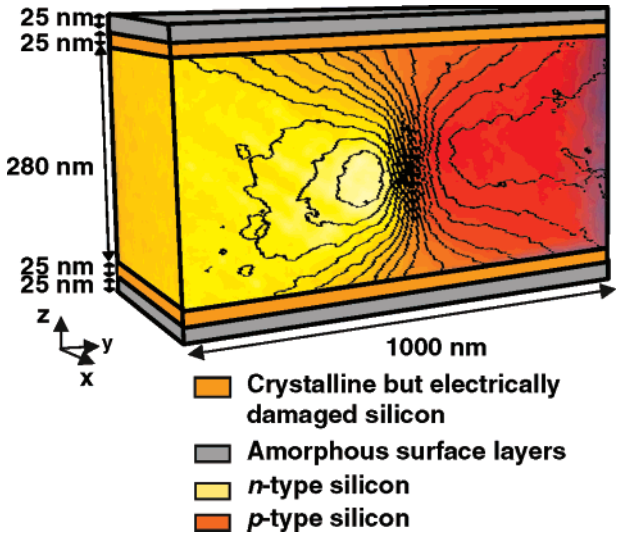

Figure 2. Tomographic reconstruction of the electrostatic potential arising from a 3-D section of a thin FIB-prepared membrane containing an electrically biased p−n junction. Substantial modification of the potential is apparent near the top and bottom surfaces of the reconstruction arising from a combination of sample preparation effects and properties of semiconductors (such as surface depletion) near surfaces. The amorphous and crystalline surface layers have been represented schematically and were not reconstructed tomographically. Equipotential contours spaced every 0.2 V have been superimposed onto the reconstructed tomogram, highlighting the electrostatic potential distribution in the $y-z$ cross-section of the specimen.

of the p−n junction were acquired in a Philips CM300 field emission gun TEM using an accelerating voltage of 200 kV over a tilt range of −70 to +70°, with holograms acquired at 2° intervals. Reference holograms from vacuum were acquired every 10°. Phase images (Figure 1c) were reconstructed numerically using reference holograms to remove artefacts resulting from the image recording process.[13] Phase unwrapping procedures were used with care to ensure that the total phase change of the electron wave was recovered, relative to a wave passing through vacuum alone. The electrostatic potential revealed in the reconstructed phase image is a projection through the membrane and contains contributions from both surface and bulk regions. By using tomography in combination with electron holography, the 3-D variation in electrostatic potential (as illustrated schematically in Figure S1, Supporting Information[5]) can be quantified, and the impact of different surface conditions on the device properties in the thin specimen can be assessed. A multiplicative iterative back-projection method[14] was used to reconstruct the 3-D electrostatic potential from the tilt series of holograms. The missing wedge of information arising from the limited tilt led to uncertainty in the precise position of the specimen surfaces perpendicular to the electron beam direction. As the FIB-prepared specimen surfaces are known to be equipotentials,[9] the reconstruction was therefore constrained to lie within the (independently measured) specimen thickness, setting the potential outside the specimen to zero.

Figure 2 shows the reconstructed 3-D electrostatic potential in the specimen, measured under an applied reverse bias voltage of 3 V, which reveals a potential distribution of the same form as that predicted by simulations.[15] A three-dimensional visualization of the tomogram is provided in the supporting online material. Only the region of varying electrostatic potential has been reconstructed tomographically (as illustrated in Figure S1, Supporting Information), excluding the amorphous and crystalline regions, which contain invariant, electrically inactive material at the top and bottom surfaces of the FIB-prepared specimen. The damage created by the Ga^+ ion beam results in the fact that the material within 25 nm of the specimen surfaces is no longer crystalline[8,9] and within 50 nm of the surface does not vary electrically as a function of position along the specimen surface. Although these surface regions do contribute to the

total phase shift of the electron beam passing through the specimen, there is no local variation in phase arising from the presence of electrically active dopants (from p- to n-type), i.e., these regions are essentially intrinsic and give rise to little information in the reconstructed tomogram. The final thickness of the tomographic reconstruction was therefore constrained to the central 280 nm of the specimen, which would correspond to the membrane having a crystalline, but electrically inactive surface layer of 25 nm (in addition to a 25 nm thick amorphous layer) at each surface,[9] as illustrated in Figure 2. The spatial and phase resolution of the holographic phase images are controlled by the acquisition and processing parameters;[16] here, the spatial resolution of the reconstructed phase images has been limited to 25 nm to improve the phase resolution. The spatial resolution in the tomogram is 25 nm in the $x-y$ plane, and 40 nm in the z-direction, with a corresponding electrostatic potential resolution of 0.2 V.[5,16] The potential distribution can be assessed quantitatively to examine the effect of the specimen surfaces by extracting information from voxels at defined distances from the membrane surface. In particular, line traces taken across the p−n junction, which are shown in Figure 3a, can be used to assess the depletion width and built-in potential across the junction as a function of position within the specimen.

In Figure 3a, the potential profiles across the p−n junction adjacent to the electrically inactive (but crystalline) near-surface layers ("top" and "bottom") show a very slowly varying electrostatic potential across the junction. In contrast, the middle of the specimen shows electrostatic behavior that is characteristic of a p−n junction in a bulk semiconductor.[5] The width of the charge separation region (marked W in Figure 3a) is expected to increase as the electrically active dopant concentration decreases. The very slow variation in electrostatic potential observed at the surfaces of the reconstructed volume therefore corresponds to the central section of the charge separation region in this part of the specimen, and the expected variation over a larger field of view is illustrated in the schematic inset shown in Figure 3a. The traces in Figure 3a show that there is a significant reduction in the concentration of charge carriers near the top and bottom of the reconstruction, corresponding to an electrically active charge concentration that is much lower than that measured in the middle of the specimen. The potential difference measured across the junction in the middle of the specimen is 3.8 ± 0.2 V, which is consistent with the theoretical built-in voltage plus the 3 V applied reverse electrical bias. Poisson's equation can be used to calculate the electric field and the electrically-*active* dopant concentration from each measured potential profile. Figure 3b shows that the electric field in the middle of the membrane is consistent with that predicted for a bulk Si p−n junction to within experimental error. The electric field at the top and bottom of the electrically active region is negligible. The scatter in the points in Figure 3b is relatively large due to the need to differentiate the experimental potential profile to derive the electric field profile. Table 1 shows a comparison of the experimentally determined values for the

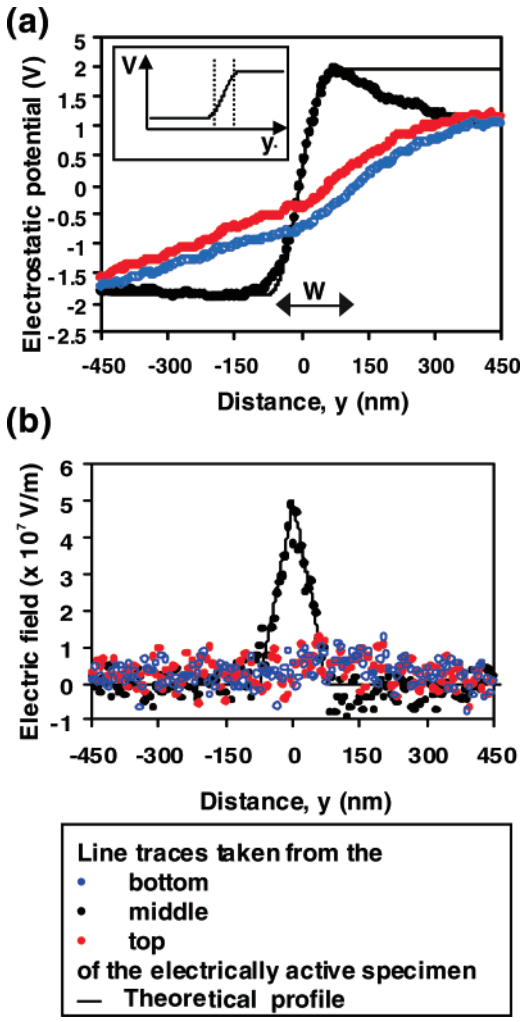

Figure 3. (a) Line profiles of the electrostatic potential variation across the junction extracted from the tomographic reconstruction acquired at a 3 V reverse bias, quantifying the change in electrostatic potential across the junction at the middle, top, and bottom of the electrically active region within the FIB-prepared membrane. The inset schematic illustrates the potential variation predicted for the "top" and "bottom" traces over a larger field of view. The variation in electrostatic potential for an ideal, abrupt junction symmetrically doped with an active concentration of 4.5×10^{17} cm^{-3} is shown for comparison. (b) Line profiles of the electric field (calculated from the potential distribution using Poisson's equation) associated with the electrically biased p−n junction at the middle, top, and bottom of the electrically active region within the FIB-prepared membrane. The theoretical profile for an active dopant concentration of 4.5×10^{17} cm^{-3} is shown for comparison.

charge density and electric field with theoretical calculations for an abrupt p−n junction in a bulk semiconductor that is doped symmetrically with an electrically active dopant concentration of 4.5×10^{17} cm^{-3}. These results show that the electrically active dopant concentration for the biased p−n junction in the middle of the specimen is $4.5 \pm 2 \times 10^{17}$ cm^{-3}, with the electrically active dopant concentration dropping to zero at the top and bottom surfaces of the reconstructed volume. The best-fitting value for the electrically active dopant concentration for the unbiased specimen is lower than that for the 2 and 3 V electrically biased results, as observed previously, for reasons that are not yet fully understood.[17]

Table 1. Comparison of Quantitative Experimental Results Obtained from the Middle of Tomographic Reconstructions of the Electrostatic Potential Associated with a FIB-prepared Si p−n Junction with Theoretical Calculated Values for an Abrupt, Bulk Si p−n Junction with the Active Dopant Concentration Defined in the Table

applied electrical bias (V)	charge density ($\times 10^{17}$ cm^{-3})		electrostatic potential (V)		maximum electric field ($\times 10^{7}$ Vm^{-1})	
	theor	exptl	theor	exptl	theor	exptl
0	2	2 ± 2	0.89	0.74 ± 0.2	1.6	1.3 ± 1
2	4.5	4.5 ± 2	2.89	2.66 ± 0.2	4.4	3.7 ± 1
3	4.5	4.5 ± 2	3.89	3.83 ± 0.2	5.15	4.9 ± 1

The application of tomographic electron holography to semiconductor devices promises to provide essential quantitative 3-D information about potential distributions in complex nanometer-scale semiconductor structures. This information is particularly important for structures such as semiconductor nanowires or ribbons,[18] where surface and interfacial properties may dominate the electrical behavior of the device. Further experiments on specimens of different thickness are required to investigate whether the results presented here represent the bulk properties of this wafer, and to determine the thickness that must be used for future experiments to ensure that bulk-like behavior is present in the membrane center. Recently, in situ annealing of Si specimens has been shown to improve the measured electron holographic phase signal due to the removal of Ga-induced defects and damage.[19] The examination of pre- and post-annealed Si specimens using tomographic holography would help further the understanding of the effects of Ga-induced defects on the electrical properties of the semiconductor. A reduction in the thickness of surface damage layers by low-energy ion milling will also be investigated in a future study.

Acknowledgment. This work was supported by Newnham College, Cambridge, the Royal Society, the EPSRC, FEI Company, and the IP3 project of the 6th Framework Programme of the European Commission: Enabling Science and Technology for European Electron Microscopy (ESTEEM) contract no. 0260019. We thank Philips Research Laboratories, Eindhoven, for providing the doped silicon wafer.

Supporting Information Available: Materials and methods, figures, references, movie (AVI). This material is available free of charge via the Internet at http://pubs.acs.org.

References

(1) Semiconductor Industry Association roadmap 2005 update http://public.itrs.net/.
(2) Roy, S.; Asenov, A. *Science* **2005**, *309*, 388.
(3) Castell, M. R.; Muller, D. A.; Voyles, P. M. *Nat. Mater.* **2003**, *2*, 129.
(4) Frank, J. *Electron Tomography: Three-Dimensional Imaging with the Transmission Electron Microscope*, Plenum Press: New York, 1992.
(5) See Supporting Information for further details.
(6) Bicais-Lepinay, N.; Andre, F.; Pantel, R.; Jullian, S.; Margain, A.; Kwakman, L. F. T. *Microelectron. Reliab.* **2002**, *42*, 1747.
(7) de Veirman, A. E. M. *Mater. Sci. Eng. B* **2003**, *102*, 63.
(8) Rubanov, S.; Munroe, P. R. *J. Microsc.* **2004**, *214*, 213.
(9) Twitchett, A. C.; Dunin-Borkowski, R. E.; Midgley, P. A. *Phys. Rev. Lett.* **2002**, *88*, 238302.
(10) Spence, J. C. H.; Zuo, J. M. *Electron Microdiffraction*; Plenum Press: New York, 1992.
(11) E. A. Fischione Instruments, Inc., www.fischione.com.
(12) Dunin-Borkowski, R. E.; Twitchett, A. C.; Barnard, J. S.; Broom, R. F.; Midgley, P. A.; Robins, A. C.; Smith, D. W.; Gronsky, J. J.; Fischione P. E. *Microsc. Microanal.* **2004**, 10, 1012.
(13) Volkl, E.; Allard, L. F.; Joy, D. C. *Introduction to Electron Holography*; Kluwer Academic/Plenum Publishers: New York, 1999.
(14) Gilbert, P. *J. Theor. Biol.* **1972**, *36*, 105.
(15) Somodi, P. K.; Dunin-Borkowski, R. E.; Twitchett, A. C.; Barnes, C. H. W.; Midgley, P. A. *IOP Conf. Ser.* **2003**, *180*, 501.
(16) Lichte, H. *Ultramicroscopy* **1991**, *38*, 13.
(17) Twitchett, A. C.; Dunin-Borkowski, R. E.; Hallifax, R. J.; Broom, R. F.; Midgley, P. A. *Microsc. Microanal.* **2005**, *11*, 1.
(18) Ahn, J.-H.; Kim, H.-S.; Lee, K. J.; Jeon, S.; Kang, S. J.; Sun, Y.; Nuzzo, R. G.; Rogers, J. A. *Science* **2006**, *314*, 1754.
(19) Cooper, D.; Twitchett, A. C.; Somodi, P. K.; Midgley, P. A.; Dunin-Borkowski, R. E.; Farrer, I.; Ritchie, D. A. *Appl. Phys. Lett.* **2006**, *88*, 063510.

NL070858N